Development of CFD Capability for Full Helicopter Engineering Analysis

G. Barakos[1], R. Steijl[2], K. Badcock[3] and A. Brocklehurst[4]

[1-3]CFD Laboratory
Dept. of Aerospace Engineering
University of Glasgow
Glasgow G12 8QQ
United Kingdom

[4]Rotor Aerodynamics
Rotor Systems Group
Westland Helicopters
Yeovil, BA20 2YB
United Kingdom

Abstract

This paper presents the development and validation of a CFD method suitable for analysing the flow around a complete helicopter. Emphasis is placed on the detailed validation for a range of flow cases designed to assess the predictive capability of the method. Several fundamental flow cases are presented including tip flows, blade-vortex interaction and three-dimensional dynamic stall. Solutions for isolated rotors are also obtained both at hover and forward flight conditions. The detailed validation of the method for fundamental flows was found to be beneficial when more complex cases were considered like the flow around a helicopter fuselage or the rotor/fuselage interaction. Throughout, experimental data available in the public domain has been used and a substantial validation database has been compiled. Overall, the method was found capable of capturing the basic flow characteristics, however, the need for detailed experimental data has been identified as a number one priority in order to assess the method in predicting the interactions between the main rotor the fuselage and the tail rotor at a wide range of conditions.

Introduction

In contrast to CFD solutions for complete fixed-wing aircraft, which appear frequently in the literature, the case of a full helicopter still remains rare [1,2,3]. There are several reasons for this, the main being the complexity of the flow around a helicopter which can challenge modern CFD methods even when the conditions considered are well within the design envelope. A summary of the flow phenomena associated with helicopter flows can be found in the review paper by Conlisk [3] and is discussed in detail in specialised rotorcraft textbooks [4,5,6,7]. For this work three fundamental flow phenomena have been identified as key for CFD validation. These include the formation of the tip vortex [8-9], the three-dimensional dynamic stall [10-11] and the blade-vortex interaction [12-13]. In addition, the CFD analysis of the flow around isolated rotors in hover and forward flight conditions requires specific formulation of the governing equations to account for the rotation and the actuation of the blades which is not the case for the fixed-wing problem. For this work several flow cases have been considered based on public-domain experimental data [14-18].

1 Senior Lecturer, gbarakos@aero.gla.ac.uk
2 Post-Doctoral Research Associate
3 Reader
4 Principal Engineer, PhD Candidate

Contrary to the fixed-wing problem, the deflection of the blades during flight is a fundamental part of the problem making it difficult to distinguish between the aerodynamic and aeromechanics aspects. Detailed analysis and careful trimming of the rotor is thus required [19-22] if comparisons are to be made against experiments.

Finally, the flow around the helicopter fuselage is a fundamentally different problem than those discussed above since it has strong bluff-body characteristics which contrasts with the flow around the rotor. For this work the CFD method has been tested against experimental data for the ROBIN body [23-24]. The same body has been used as the basis for assessing the capability of the current CFD method for the rotor-body interaction problem.

Results have been obtained for several flow cases ranging from the fundamental flows discussed in the previous paragraphs, to isolated rotors and further to rotor/body interaction. Comparisons against data from experiments were used in order to assess the CFD method, the employed grids and turbulence models. Finally, conclusions from this exercise are drawn and future steps are highlighted.

Numerical Method

The CFD method summarised in [25] and further extended and utilised for rotor flows in [26] forms the basis of this work.

The code is capable of solving flow conditions from inviscid to fully turbulent using the Reynolds Averaged Navier-Stokes (RANS) equations in three dimensions. Detached eddy simulation and large eddy simulation options are also available. One- and two-equation turbulence models are available for RANS simulations and these represent a good compromise between accuracy and efficiency for most of the flow cases considered in this work. To solve the RANS equations, multi-block grids were generated around the required geometries, and the equations were discretised using the cell-centered finite volume approach. For the discretisation of the convective fluxes, Osher's scheme has been used. A formally third order accurate scheme is achieved using a MUSCL interpolation technique. Viscous fluxes were discretised using central differences. Boundary conditions were set using two layers of halo cells. The solution was marched in time using an implicit second-order scheme and the final system of algebraic equations was solved using a pre-conditioned Krylov subspace method.

In addition to the above, the motion of the blades due to rotation, pitch, flap and lead-lag has to be accounted for and this is done via grid deformation with the exception of the rotational motion. To deform the CFD grid the trans-finite interpolation (TFI) method has been employed. Figure 1a shows a rotor blade surrounded by a set of blocks which are designed to move with it undeformed. All other blocks in the grid are allowed to deform using the TFI method. It was found [26] that this hybrid technique resulted in better grid quality for the simulations in comparison to pure TFI.

The sliding plane concept is used to allow rotor/body simulation. According to this method the grid around the fuselage stays fixed (See Figure 1b) while the grid surrounding the rotor blades is allowed to rotate. Communication between the two grid sets is done via a sliding plane which in effect is a part of computer memory where an interpolated solution is constructed using information from the grids on the adjacent sites. This technique has been used in the past in turbomachinery computations (see ref 27 for example) and good accuracy has been reported.

Results and Discussion

In the following paragraphs results are presented for a wide range of cases assessing the ability of the solver. Fundamental and complex flows have been considered.

Fundamental Flows

The flow around a blade tip and the formation of the tip vortex, dynamic stall in 3D and head-on parallel blade-vortex

interaction cases have been considered. The results presented in this paper represent only a small fraction of the cases studied which are now part of the validation database of the CFD solver.

Tip flow

The current CFD method has been validated against experimental data of the velocity field behind wing tips at steady and unsteady flow conditions. Figure 2a presents a comparison between CFD and experiments by Margaris [8] for the streamwise velocity component behind a NACA 0015 wing at a fixed incidence of 10 degrees. This detailed experimental investigation provided high fidelity data necessary for CFD validation using a PIV system. As can be seen, the velocity magnitude is well predicted and the same can be said about the location of the tip vortex. For the CFD computations, a fine grid of more than 600 thousand cells had to be used in order to capture the details of the rollup of the vortex and preserve its structure downstream. For unsteady flow conditions, the work of Ramaprian et al [9] has been used. Figure 2b presents the comparison between experiments and CFD for the flow field near the tip at various phases during the oscillation of the wing. The position of the wing's trailing edge is denoted by the dashed line and as can be seen the position of the vortex is accurately captured. In comparison to the previous set of data it should be noted that the matrix of measurements behind the wing is sparse. For this case the laser had to be moved to cover the whole flow field and consequently the results are of lesser resolution on comparison to the PIV close to the tip. Again, fine CFD grids of about 500 thousand points had to be used. For all cases a variety of turbulence models of the k-omega family were used and the transition point was fixed as indicated by the experiments.

BVI

In contrast to the previous cases where the tip vortex is continuously fed by the pressure difference between the two sides of the wing, blade/vortex interaction cases show a greater dependence on the employed grids and numerical schemes. To counter the excessive numerical dissipation and dispersion associated with relatively coarser grids the current CFD solver was modified to include the vorticity confinement method [28]. The details of the implementation are given in the recent paper by Morvant *et al.* [13] and results are shown here for subsonic (Figures 3a,3b) and transonic (Figure 3c) parallel BVI cases simulated as two dimensional interactions between a vortex and a blade section. The experiments by Lee and Bershader for a NACA section at zero incidence were used for validation and indicative results are presented in Figures 3a and 3b. As can be seen, the confinement method was found to be adequate for simulating this case and the results obtained for the history of the surface pressure distribution are in good agreement with measurements. It has to be noted that without the vorticity confinement method grids of about 200 thousand points were found to be inadequate for simulating the BVI since the core of the vortex was sensitive to the numerical scheme employed. However, even at transonic flow conditions (Figure 3c) the current method was able to track the vortex during its interaction with both the aerofoil and the shock present. As can be seen the vortex persists after surviving the interaction with the shock and continues along its path, passing just below the blade section.

Dynamic stall

In addition to the tip flow and the BVI the phenomenon of dynamic stall was also studied. In contrast to most of the works found in the literature dynamic stall was studied in 3-D. Several cases have been considered for validation and a detailed account of the 3D dynamic stall flow can be found in the recent paper by Spentzos *et al.* [29]. Emphasis was put on comparisons against modern experimental data obtained using optical techniques. Such data have been provided by the work of Berton *et al.*

[10] and a comparison is shown in Figure 4a. The detailed comparisons shown in the figure indicates that the evolution of the dynamic stall phenomenon is well captured and the formation and growth of the dynamic stall vortex are well represented by the CFD method. The size of the separated flow region is always well-predicted for this case at all location on the oscillating wing and for all phases of the phenomenon. In addition to this comparison, the experimental data by Coton and Galbraith of Glasgow University [11] were also used and comparison against CFD results for the surface pressure distribution is shown in Figure 4b. The characteristic foot-print of the dynamic stall vortex on the surface pressure is well captured. Due to the complexity of the phenomenon and the rapid development of the dynamic stall, refinement of the time-step used for the CFD was found to be a key factor with up to 500 steps required per oscillation cycle if accurate results are needed. Again, linear and non-linear turbulence models of the k-omega family have been used along with fixed transition.

Isolated Rotors
A second set of validation cases considered isolated helicopter rotors in hover and forward flight. The key challenge was to obtain accurate results with the minimum possible CPU time.
As explained in the numerical method section, the rotor blades are surrounded by rigid blocks of cells to allow for adequate prediction of the surface pressure. Deforming grids are used to allow the blades to move. In total, validation results for about fifteen model rotors have been obtained and only a small fraction is shown here. Studies using the Caradonna-Tung [17] rotor were first conducted in order to establish the required grid density and multi-block topology. Although emphasis is placed on the accurate prediction of the surface loading the grids were also refined in the wake region in order to capture the rotor wake. Figure 5a presents results of the wake behind a hovering Caradonna Tung

rotor for two grid densities. As can be seen about 4 million cells are needed in order to capture the second revolution of the wake spiral. The position of the vortex was accurately captured as can be seen in Figure 5b where CFD predictions are compared against experiments [16] for the wake of the UH-60A rotor. It is remarkable that good accuracy can be obtained even on grids of about 1.5 million points per blade. Using data for the same rotor [16] the accuracy of the solver in prediction the loads in hover has been assessed. Figure 6 compares the predicted surface pressure for a hovering case against the experimental data. For this case, grids of 1.5 million points per blade were used and although the calculations were conducted for an inviscid model the thrust coefficient was well predicted and encouraging results have also been obtained for the torque. Several other comparisons using the ONERA model rotors or the ONERA 7A/7AD blades [14] resulted in similar conclusions. In the literature a wide range of cases is available for isolated model rotors which can be used for validation of CFD codes. It is, however, evident that surface pressure measurements combined with integrated load measurements and wake surveys are rare. As experimental techniques advance and accurate PIV and LDV/LDA data is obtained for unsteady flows further validation will be carried out.

Flow around fuselage
Heading towards CFD simulation of a complete helicopter the solver was first validated against experimental data for flow around an isolated fuselage. Such data are available for the ROBIN body by an extensive experimental campaign at NASA [23,24]. A multi-block grid was constructed around the body and the rotor pylon. The grid density was in excess of 1 million points for the half-model of the ROBIN body and a complex multi-block topology was devised so that the exact shape could be represented. Several validation cases have been considered with the flow at 0, ±5 and ± 10 degrees of incidence. Mild separation was detected behind the pylon and as can be

seen from Figure 7. The CFD results for the surface pressure are in fair agreement with experiments for all stations where pressure taps were available during the experiment. Although this comparison is encouraging little can be said about the integrated loads predicted by the CFD due to lack of adequate data for validation. The same is true for the wake of the fuselage. Clearly data of higher fidelity are needed like that obtained during recent experimental campaigns [30-31].

Rotor Body Interaction
As a final demonstration, simulation of the flow around the ROBIN body [23] placed below the HIMARCS rotor [15] has been attempted. There are no experimental data available for this case and it has therefore only been used as a demonstration for the complete CFD capability developed by the authors. For this case the rotor blades were at a fixed collective (2 degrees) and zero cyclic, the objective being the assessment of the performance of the sliding plane placed between the rotor and the body. Figure 8a presents the overall configuration while Figures 8b and 8c present the complex multi-block topologies employed for the rotor blades and the fuselage, respectively. The final grid was in excess of 6 million points and it is considered to be coarse for the rotor blades. In total 465 blocks were used to mesh the whole geometry and a snap-shot of the flow field can be seen in Figure 8d. It is evident from the streamlines drawn that the flow field around the fuselage is distorted due to the presence of the rotor. Unfortunately rotor/body interaction data suitable for CFD are rare in the open literature and efforts are now directed towards a detailed validation of the solver using cases reported in [30-31] as well as the expected data of the GOAHEAD project.

Conclusions and Future Steps
The objective of this work was to describe the steps taken towards the development of a CFD solver capable of accurately and efficiently simulating flows pertinent to helicopters including a full helicopter capability.

This difficult task required a step-by-step approach with careful validation and assessment of each key component against the best available experimental data. The key identified steps were: (a) development of an efficient solver, (b) validation for key aerodynamic phenomena pertinent to rotors (dynamic stall, blade-vortex interaction, flow separation, shock- boundary-layer interaction, bluff body flow etc), (c) development of grid motion and deformation algorithms able to cope with all rotor blade motions and aeromechanic requirements and (d) development of a sliding-grid capability to allow for rotor/body simulation.

References
1. Pahlke, K. and B.G. van der Wall, Chimera Simulations of Multibladed Rotors in High-speed Forward Flight with Weak Fluid-structure Coupling, *Aerospace Science and Technology*, **9** 379–389, 2005.
2. O'Brien, D.M. Jr and Smith, M.J., Analysis of Rotor-Fuselage Interactions Using Various Rotor Models, AIAA 43nd Aerospace Sciences Meeting, *AIAA 2005-0468*, Reno, NV January 10-13, 2005.

3. Conlisk, A., Modern Helicopter Aerodynamics, Annual Review of Fluid Mechanics, Vol. 29, 1997, pp. 515-567.

4. Bramwell, A.R.S., Helicopter Dynamics. (1 st ed.), Edward Arnold, London, 1976.

5. Seddon, J. Basic Helicopter Aerodynamics. (1st ed.), BSP Professional books, Oxford, 1990.

6. Newman, S. The foundations of Helicopter Flight, Arnold, London, 1994.

7. Nikolsky, A.A. Helicopter Analysis, John Wiley & Sons, New York, 1951.

8. Margaris, P. and Gursul, I., Effect of Steady Blowing on Wing Tip Flow Feld,Technical report, University of Bath, 2004.

9. Ramaprian, B. and Cheng, Y., Near Field of the Tip Vortex Behind an Oscillating Rectangular Wing. *AIAA Journal*, **36**(7), 1263.1269, 1998.

10. Berton E., Allain C., Favier D. and Maresca C., Experimental Methods for Subsonic Flow Measurements, in Progress in Computational Flow-Structure Interaction, Haase W., Selmin V. and Winzell B., Eds., Notes on Numerical Fluid Mechanics and Multidisciplinary Design, Vol 81, Springer, 97-104, 2003.

11. Coton, F.N. and Galbraith, R.A.M., An Experimental Study of Dynamic Stall on a Finite Wing, *Aeronautical Journal*, **103**(1023), 229-236, 1999.

12. Lee, S., and Bershader, D., "Head-On Parallel Blade-Vortex Interaction," *AIAA Journal*, **32**(1), 16–22, 1994.

13. Morvant, R., Badcock, K.J., Barakos, G.N. and Richards, B.E., Aerofoil-Vortex Interaction Using the Compressible Vorticity Confinement Method, *AIAA J.* **43**(1), 63-75, 2004.

14. Philippe, J-J. and Chattot, J-J. Experimental and theoretical studies on helicopter blade tips at ONERA. Sixth European Rotorcraft and Powered Lift Aircraft Forum, Bristol, September 16-19, 1980.

15. Noonan, K.W., Yeager, W.T., Singleton, J.D., Wilbur, M.L., and Mirick, P.H. Wind Tunnel Evaluation of a Helicopter Main-Rotor Blade with Slotted Airfoils at the Tips. Technical report, NASA Langley Research Centre, *NASA-TP-2001-211260*, December 2001.

16. Kufeld, R. and Bousman, W., UH-60A Airloads Program Azimuth Reference Correction, *J. American Helicopter Society*, **50**, (2), 211-213, 2005.

17. Caradonna, F.X. and Tung, C. Experimental and Analytical Studies of a Model Helicopter Rotor in Hover. Technical report, NASA Technical Memorandum *TM-81232*, 1981.

18. Schultz, K.J., Splettstosser, W., Junker, B., Wagner, W. and Arnaud, G., A Parametric Windtunnel Test on Rotorcraft Aerodynamics and Aeroacoustics (Helishape) - Test Procedures and Representative Results, *Aeronautical Journal* **101**(1004), 143-154, 1997.

19. Pomin, H. and Wagner, S. Navier-Stokes Analysis of Helicopter Rotor Aerodynamics in Hover and Forward Flight, *Journal of Aircraft*, **39**(5), 813-821, 2002.

20. Pomin, H. and Wagner, S. Aeroelastic Analysis of Helicopter Rotor Blades on Deformable Chimera Grids, *Journal of Aircraft*, **41**(3), 577-584, 2004.

21. Servera, G., Beaumier, P., Costes, M., A Weak Coupling Method between the Dynamics Code HOST and the 3D Unsteady Euler Code WAVES, *Aerospace Science and Technology,* **5**, 397-408, 2001.

22. Park, Y. and Kwon, O., Simulation of Unsteady Rotor Flow Field using Unstructured Adaptive Meshes, *Journal of the American Helicopter Society,* **49**(4):391-400, 2004.

23. Mineck, R.E. and Althoff, S., Steady and Periodic Pressure Measurements on a Generic Helicopter Fuselage Model in the Presence of a Rotor, NASA/*TM-2000-210286*, 2000.

24. Chaffin, M.S., and Berry, J.D., Navier-Stokes and Potential Theory Solution for a Helicopter Fuselage and Comparison with Experiments, NASA Technical

Memorandum *TM-4566*, Langley Research Centre, June 1999.

25. Badcock, K., Richards, B. and Woodgate M. Elements of Computational Fluid Dynamics on Block Structured Grids Using Implicit Solvers, *Progress in Aerospace Sciences*, **36** (5-6):351-92, 2000.

26. Steijl, R., Barakos, G. and Badcock, K., A Framework for CFD Analysis of Helicopter Rotors in Hover and Forward Flight, *Int. J. Num. Meth. Fluids*, July 2005.

27. Barakos, G., Vahdati, M., Sayma, A.I., Breard, C. and Imregun, M., A Fully Distributed Unstructured Navier-Stokes Solver for Large-Scale Aeroelasticity Computations, *The Aeronautical Journal*, **105**(1050), 419-426, 2001.

28. Steinhoff, J., and Underhill, D., "Modification of the Euler Equations for Vorticity Confinement: Application to the Computation of Interacting Vortex Rings," *Journal of Physics Fluid*, **6**(8), 2738–2744, 1994.

29. Spentzos, A., Barakos, G., Badcock, K., Richards, B., Wernert, P., Schreck, S. and Raffel, M., CFD Investigation of 2D and 3D Dynamic Stall, *AIAA J.*, November 2004.

30. van der Wall, B.G., Junker, B., Burley, C.L., Brooks, T.F., Yu, Y., Tung, C., Raffel, M., Hugues, R., Wagner, W., Mercker, E., Pengel., K., Holthusen, H., Beaumier, P., Dellieux, Y.: "The HART II Test in the LLF of the DNW – A Major Step Towards Rotor Wake Understanding," 28th European Rotorcraft Forum, Bristol, UK, September, 17-20, 2002.

31. Yu Y., Tung C., van der Wall B., Pausder J, Burley C., Brooks T., Beaumier P., Delrieux Y., Mercker E.: " The HART-II Test: Rotor Wakes and Aeroacoustics with Higher-Harmonic Pitch Control (HHC) Inputs- The Joint German / French / Dutch /US Project", AHS 58th Annual Forum, Montreal, Canada, June 2002.
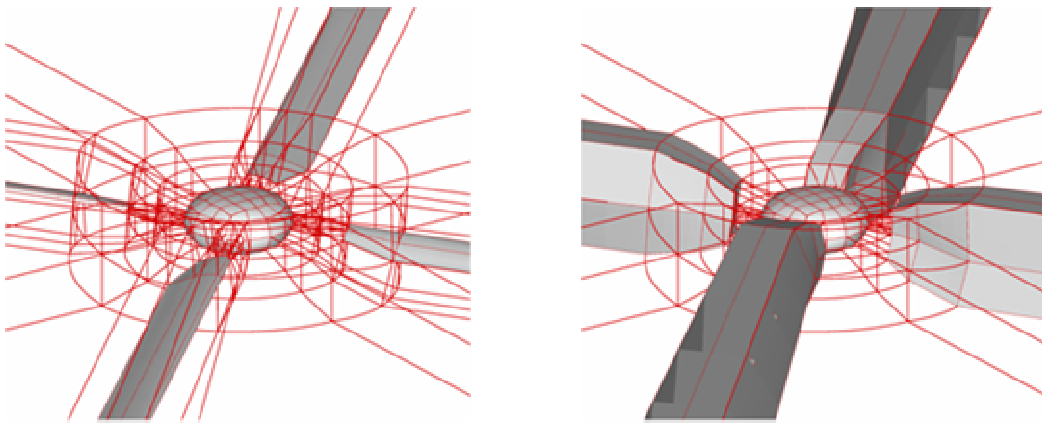
(a)
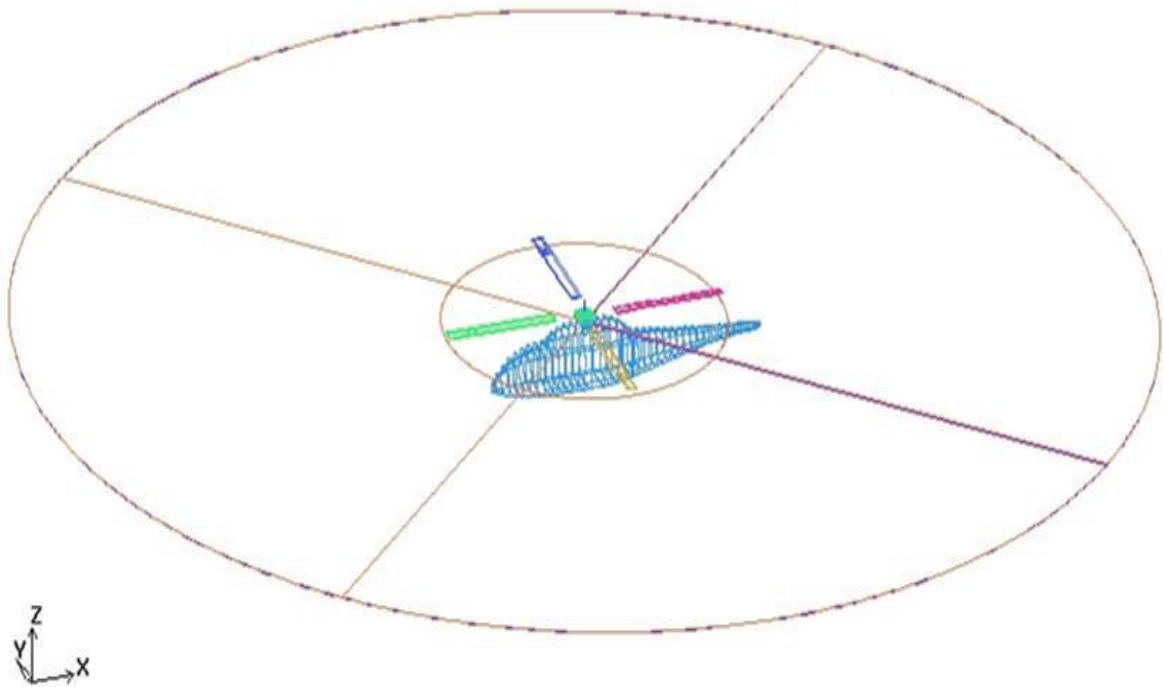
(b)

Figure 1: (a) multi-block topology for isolated rotor and (b) sliding plane between the rotor and the fuselage for rotor-body problems.
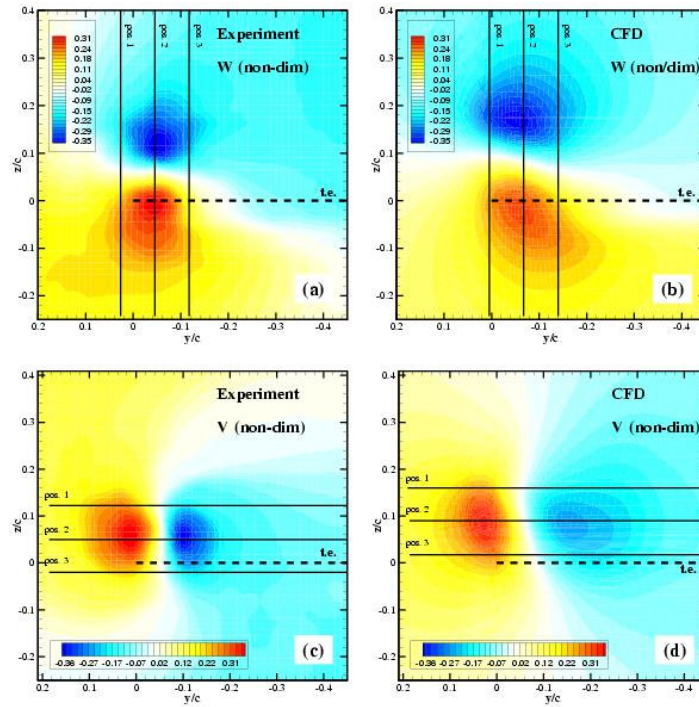
(a)
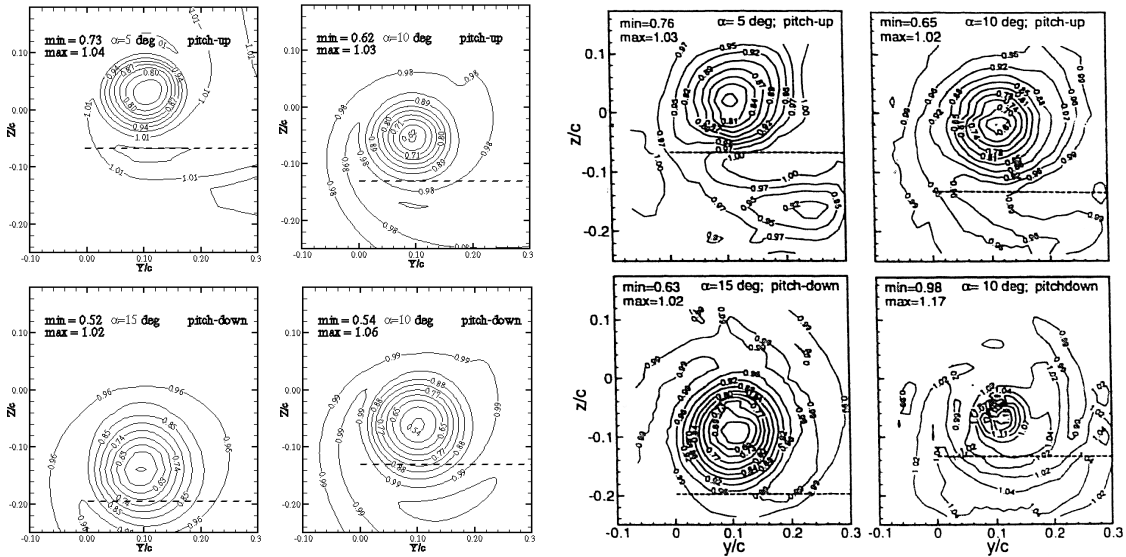
(b)

Figure 2: Comparison between CFD results and experiments for the flow behind a wing tip. (a) $M = 0.1$, $Re = 100,000$, $\alpha = 10°$, steady flow, conditions correspond to the experiments by Margaris and Gursul [8]. (b) Oscillating wing case, distance $x/c = 1.33$ behind trailing edge. Experimental data are from Ramaprian [9] ($M = 0.15$, $Re = 1.8 \times 10^5$, Incidence $\alpha = 10°$).
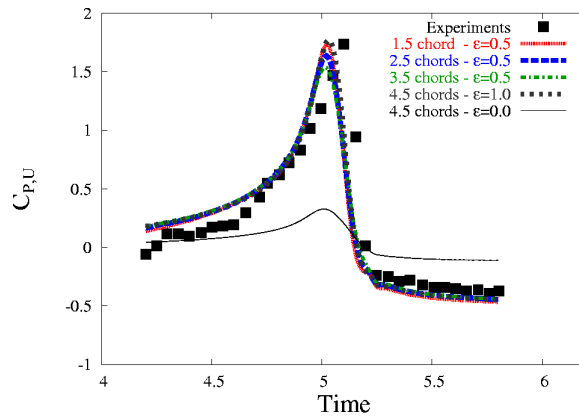
(a) Upper side (x/c=0.02)
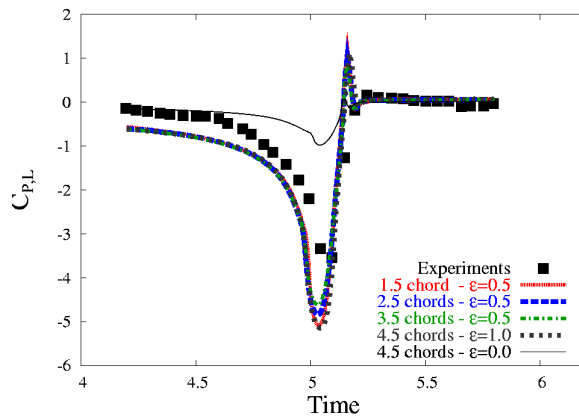
(b) Lower side (x/c=0.02)
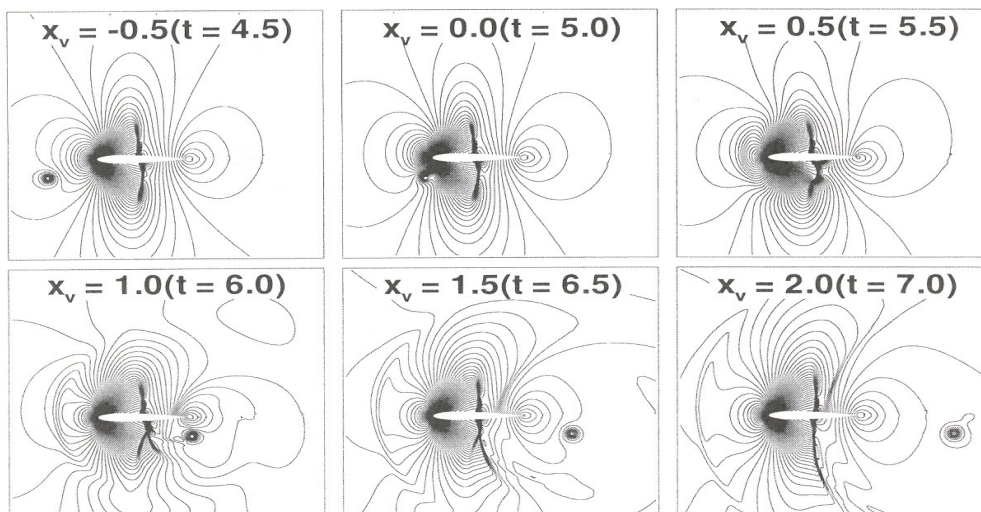
(c) Transonic interaction

Figure 3: CFD analysis of BVI using the vorticity confinement method. (a,b) subsonic parallel interaction, (c) transonic parallel interaction (case by Lee and Bershader [12], NACA -0012, zero incidence).

(a)

(b)
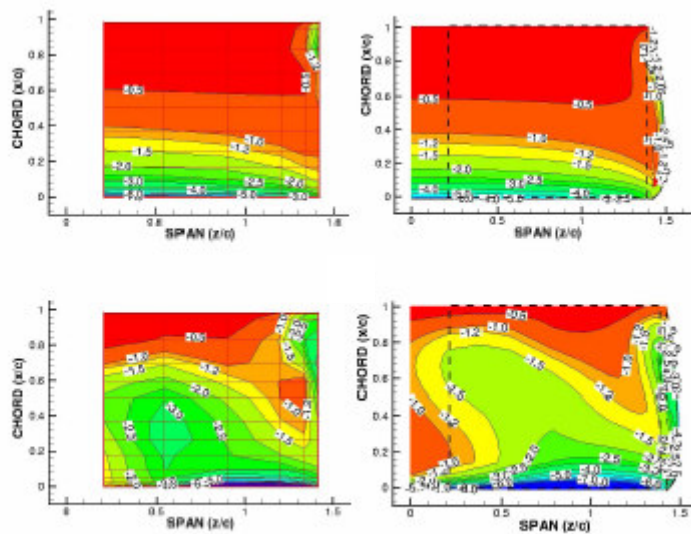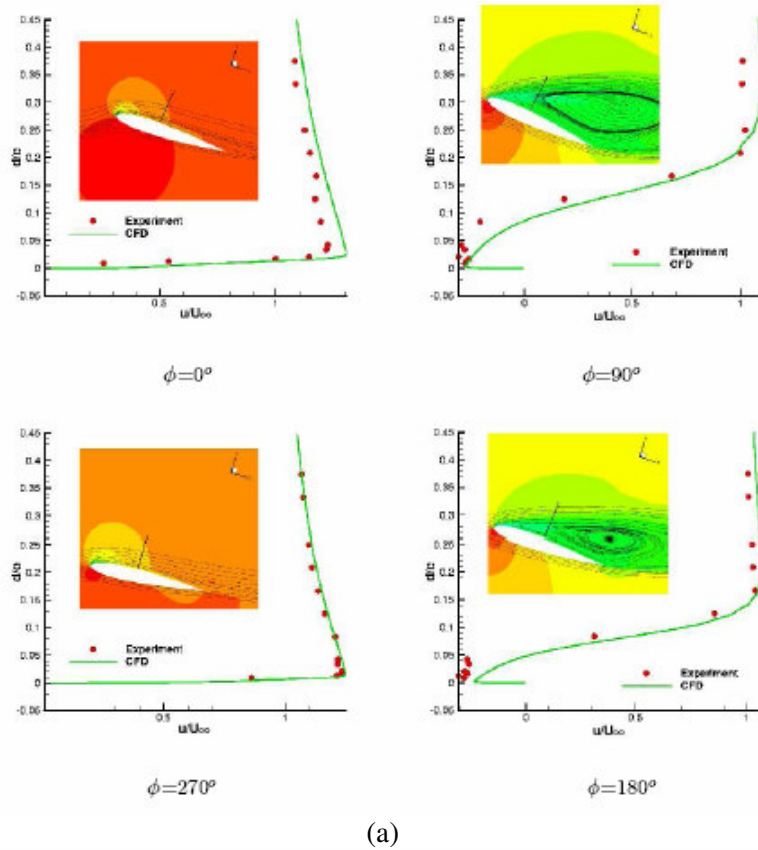
Figure 3: CFD analysis of 3D dynamic stall. (a) Velocity profiles during oscillation in pitch (Case by Berton et al. [10]). (b) Comparison between experiments (right) and CFD (left) for the surface pressure distribution over an oscillating wing. The conditions correspond to the experiments by Coton and Galbraith [11].

91.11
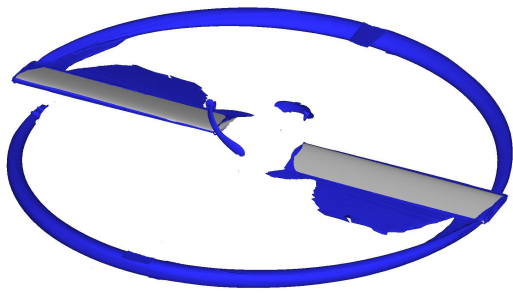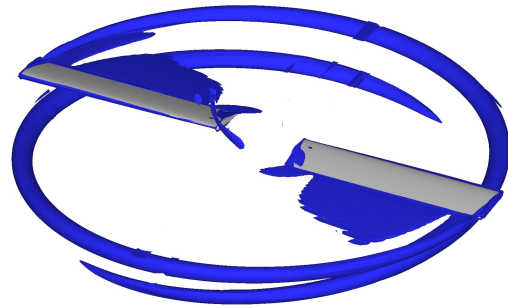
2.5 M points   4.7 M points

(a)
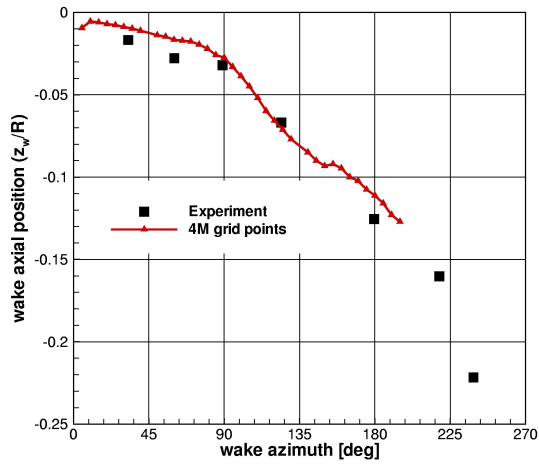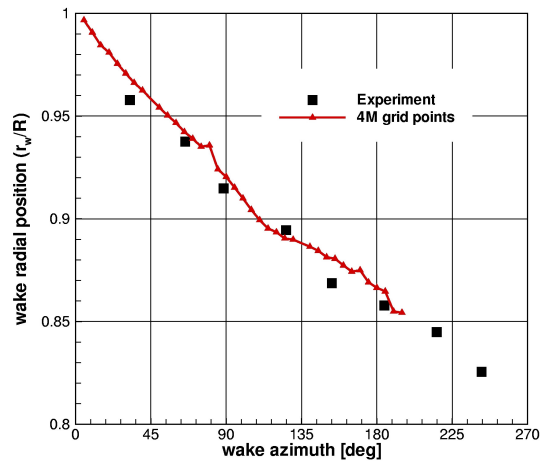
Axial position   Radial position

(b)

Figure 5: (a) Hovering Caradonna-Tung rotor [17], effect of grid density on wake resolution. (b) UH-60A rotor in hover: wake vortex position, 11.47 degrees collective pitch, M_{tip} =0.628, inviscid computation, 240-block grid, 4.5×10^6 grid points.
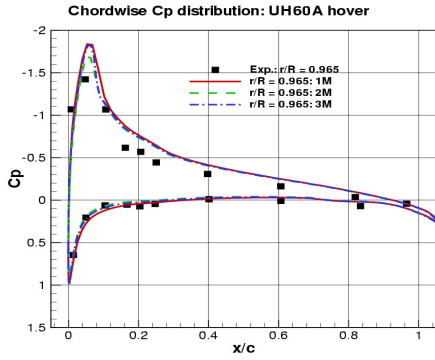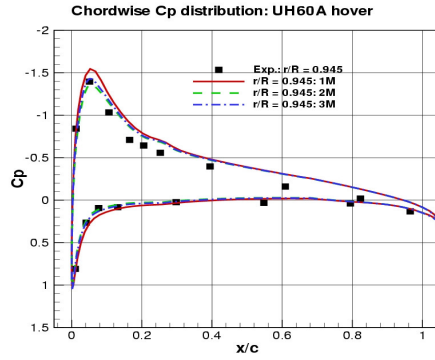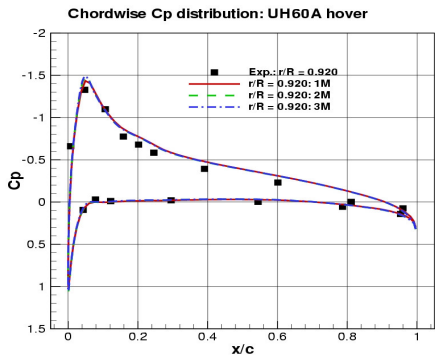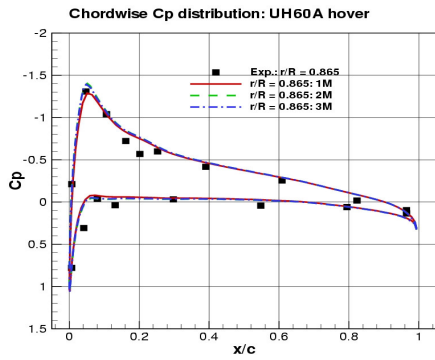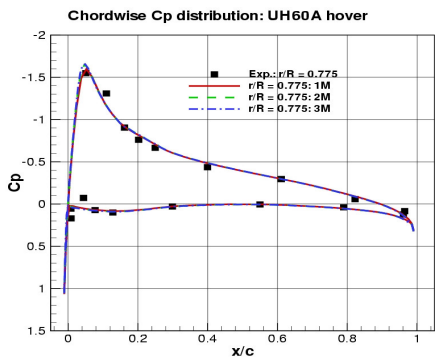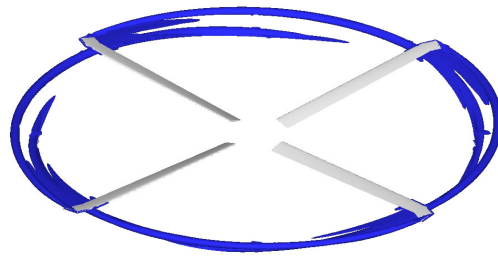
Figure 6: Comparison between CFD and experiments for the hovering UH-60A rotor. (a-e) chordwise Cp distribution at several radial stations, (f) vorticity contours near the blade tip.
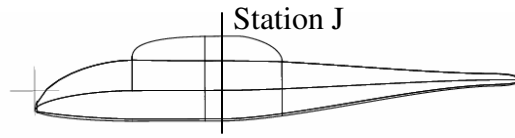
(a)
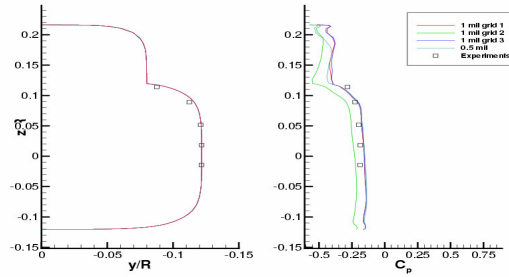
(b) 0 degrees, station J
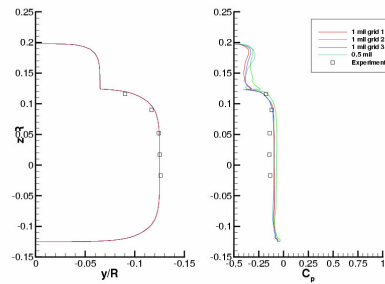
(c) 5 degrees, station J
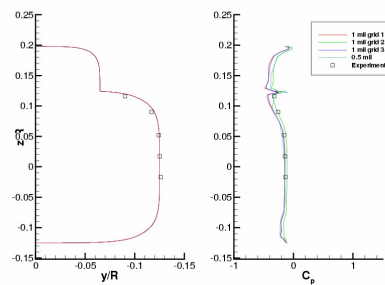
(d) -10 degrees, station J

Figure 7: Comparison between experiments [23] and CFD results for the surface pressure distribution on the ROBIN body. All CFD computations have been performed using the k-omega turbulence model.
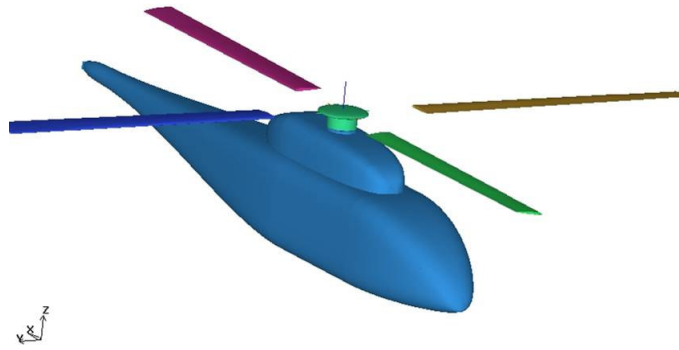
(a)
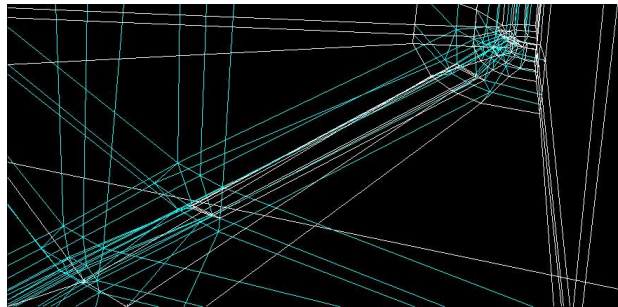
(b)
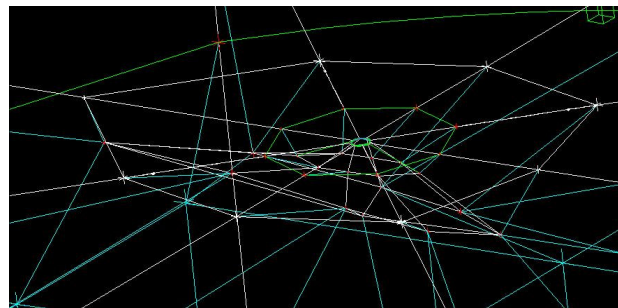
(c)
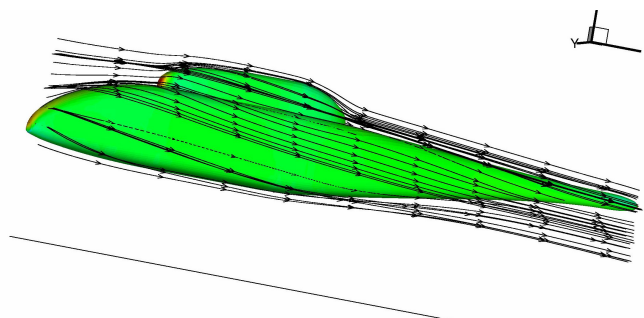
(d)

Figure 8: Rotor body configuration used for assessment of sliding planes. (a) overview of the HIMARC rotor on top of the ROBIN body (b) multi-block topology used for the rotor blades (c) multi-block topology used for the fuselage and (d) streamlines and surface pressure contours on the ROBIN body at forward flight (2 degrees of collective was used).